Journal of Structural Geology 31 (2009) 719–736

Contents lists available at ScienceDirect

Journal of Structural Geology

journal homepage: www.elsevier.com/locate/jsg

A tale of two viscosities

Mark W. Jessell [a,b,*], Paul D. Bons [c], Albert Griera [a,d], Lynn A. Evans [e], Christopher J.L. Wilson [e]

[a] Université de Toulouse, UPS (SVT-OMP), LMTG, 14 Av. Edouard Belin, F-31400 Toulouse, France
[b] IRD, LMTG, F-31400 Toulouse, France
[c] Institut für Geowissenschaften, Eberhard Karls Universität Tübingen, Sigwartstraße 10, 72076 Tübingen, Germany
[d] CNRS, LSPES, F-59655, Villeneuve d'Ascq, France
[e] School of Earth Sciences, University of Melbourne, VIC 3010, Australia

ARTICLE INFO

Article history:
Received 29 September 2008
Received in revised form
6 April 2009
Accepted 24 April 2009
Available online 5 May 2009

Keywords:
Two-phase composites
Deformation
Simple shear
SC-fabric
Shear bands

ABSTRACT

We describe a series of 12 large-strain, two-dimensional simple shear numerical experiments on two-phase linear and non-linear viscous materials. The modal percentage of the two-phases, their relative viscosities and the stress exponent of the dependence of viscosity on stress were systematically varied, allowing us to observe the effects of these parameters on the flow behaviour of the system. All experiments exhibited localisation, but the extent and type of localisation varied considerably, and the range of parameters allows both classical SC as well as SC′ structures to form.

The inter-granular finite strain geometries also varied systematically, although there is a tradeoff between non-linearity of viscosity and the viscosity contrast that results in similar geometries for quite different mechanical behaviour. The finite rotation of the harder phases was similar within any one experiment. Originally parallel passive marker lines thus remain sub-parallel after deformation and rotation, which may be mistaken for non-rotation.

The internal deformability and interaction between grains allows meta-stable grain elongation orientations to form, without any additional consideration of external slip surfaces. The slight variability of initial grain geometry and subsequent grain interactions leads to a wide variability in final grain shapes, for the same initial viscosities.

1. Introduction

The mechanical evolution of two-phase systems in rocks has been a subject of detailed field, laboratory and numerical studies, and sometimes heated debate, for several generations. These studies have in general investigated two principal subjects: the bulk mechanical behaviour of the system, and the flow field leading to the change in shape and/or rotation (or non-rotation) of the more rigid phase with respect to an external reference frame (see Table 1 for references). An improved knowledge of such composite materials is important to better constrain the mechanical predictions using homogenization techniques when used in multiscale modelling (Regenauer-Lieb et al., 2006; Liu and McVeigh, 2008).

Field observations, while crucial for constraining the type of analysis, have not in themselves resolved some of the key questions related to two-phase flow: what is the mechanical evolution to high strain? and how can we use rocks which have undergone two-phase flow as gauges for the paleo-strain tensor, stress state, or relative or absolute rheology of the phases (Passchier and Trouw, 2005, chapter 8)? The problem has been treated both in terms of the behaviour of a single more rigid object in a "soft" matrix and systems with multiple rigid objects. Whilst some physical experiments (using "natural" materials or their analogues) are able to achieve high finite strains ($>25\gamma$; e.g. Bons and Urai, 1996; Ceriani et al., 2003), numerical modelling has generally been only able to achieve quite low strains ($<2.5\gamma$; e.g. Treagus and Lan, 2003; Takeda and Griera, 2006), and has generally been limited to idealized starting configurations. Relatively few studies have addressed the behaviour of soft inclusions in a harder matrix, although a significant part of the crust consists of granitoids, where the harder feldspars provide the matrix for soft quartz inclusions.

Several studies have suggested that the effects of non-perfect bonding, interaction and the finite-length of the medium as clues to the development of stable orientations of porphyroclasts. Obviously, deformability of grains helps to develop stable orientation by development of tilted or sigma grains. An anisotropic matrix may additionally modify the rotation rate and development of stable orientations.

* Corresponding author. Université de Toulouse, IRD UPS (SVT-OMP), LMTG; 14 Av. Edouard Belin, F-31400 Toulouse, France. Fax: +33 5 61 33 25 60.
E-mail address: mark.jessell@ird.fr (M.W. Jessell).

0191-8141/$ – see front matter © 2009 Elsevier Ltd. All rights reserved.
doi:10.1016/j.jsg.2009.04.010

Table 1
Summary of studies of deformation of two-phase materials related to geology.

Reference	Approach	Single/multiple objects	Initial shape	Particle behaviour	Rheology	Objective	Max finite strain
Eshelby (1957)	Analytical	Single	Elliptical	Rigid	Elastic/viscous	Rotation	Instantaneous
Gay (1968)	Analytical	Single	Equant	Deformable	Viscous	Geom.	Instantaneous
Bilby et al. (1975)	Analytical	Single	Elliptical	Deformable	Viscous $n=1$	Geom.	Instantaneous
Ghosh and Ramberg (1976)	Analytical/physical	Single/multiple	Elliptical	Rigid	Viscous?	Rotation	$\gamma=2$
Ferguson (1979)	Physical/analytical	Single	Elliptical	Rigid	Viscous $n\geq 1$	Rotation	$\gamma=150$
Wilson (1983)	Physical	Multiple	Equant	Rigid	Viscous $n\geq 1$	Rotation	40%
Jordan (1987)	Physical	Multiple	Equant	Deformable	Complex	Mech./flow	$\gamma=5$
Burg and Wilson (1987)	Physical	Multiple	Equant	Deformable	Ice/camphor	Flow	30%
Tullis et al. (1991)	Numerical	Multiple	Equant	Deformable	Viscous $n>1$	Mech.	0.0001
Ildefonse et al. (1992)	Physical	Multiple	Elliptical	Rigid	Viscous $n>1$	Spo	$\gamma=10$
Ildefonse and Mancktelow (1993)	Physical	Multiple	Elliptical	Rigid	Viscous $n\geq 1$	Rotation/flow	$\gamma=3$
Odonne (1994)	Physical	Single	Elliptical	Deformable	Paraffin	Rotation	28%
Handy (1994)	Analytical	Multiple	Equant	Deformable	Viscous $n>1$	Mech.	Instantaneous
Bons and Urai (1994)	Physical	Multiple	Equant	Deformable	Viscous $n>1$	Flow/mech.	$\gamma=50$
Masuda et al. (1995)	Analytical	Single	Elliptical	Rigid	Viscous $n=1$	Spo	$\gamma=20$
Masuda and Mizuno (1995)	Analytical	Single	Equant	Rigid	Viscous $n=1$	Flow	$\gamma=3$
Bons and Cox (1994)	Physical/numerical	Multiple	Equant	Deformable	Elastic/viscous	Mech.	40%
Dell'Angelo and Tullis (1996)	Physical	Multiple	Equant	Deformable	Aplite	Geom./mech.	80%
Bons et al. (1997)	Numerical	Single	Equant	Rigid	Viscous $n>1$	Flow	0
Dresen et al. (1998)	Physical	Multiple	Equant	Rigid	Qtz/cte	Mech.	12%
Bruhn et al. (1999)	Physical	Multiple	Equant	Deformable	Calcite/anhydrite	Mech.	30%
Pennacchioni et al. (2000)	Numerical	Single	Equant	Rigid	Viscous $n\geq 1$	Tails	$\gamma=1$
Treagus and Lan (2000)	Numerical	Single	Equant	Deformable	Viscous $n=1$	Geom.	67%
Treagus and Treagus (2001)	Analytical	Single	Elliptical	Deformable	Viscous $n=1$	Geom.	99.9%
Mandal et al. (2001)	Numerical	Single	Elliptical	Rigid	Viscous $n=1$	Flow	4.0
Marques and Coelho (2001)	Analogue	Single	Elliptical	Rigid	Viscous $n=1$	Flow/rotation	$\gamma=7$
Mancktelow et al. (2002)	Physical	Single	Elliptical	Rigid	Viscous/lubricated $n=1$	Flow/mech.	$\gamma=15$
Piazolo et al. (2002)	Physical	Single	Circular	Deformable	elasto-viscous $n=1$	Spo	$\gamma=4$
Mancktelow (2002)	Numerical	Multiple	Equant	Deformable	Viscous $n\geq 1$	Flow	$\gamma=1$
ten Grotenhuis et al. (2002)	Physical	Single	Elliptical	Rigid	Mohr-coulomb, viscous $n=1$		
Treagus (2002)	Analytical	Single	Equant	Deformable	Viscous $n=1$	Mech./flow	75%
Ceriani et al. (2003)	Physical	Single	Elliptical	Rigid	Viscous/lubricated $n=1$	Rotation	$\gamma=45$
Treagus and Lan (2003)	Numerical	Single	Equant	Deformable	Viscous $n=1$	Geom.	$\gamma=2.7$
Taborda et al. (2003)	Numerical	Single	Elliptical	Rigid	Viscous	Rotation	$\gamma=5$
Mandal et al. (2003)	Physical	Multiple	Elliptical	Rigid	Viscous	Rotation	$\gamma=1$
Ji et al. (2004)	Analytical	Multiple	Equant	Deformable	Elastic	Mech./flow	Instantaneous
Schmid and Podladchikov (2004)	Numerical	Single	Elliptical	Rigid	Viscous	Rotation	$\gamma=1$
Johnson et al. (2004)	Numerical	Multiple	Rectangular	Deformable	Mohr-coulomb	Flow	0.0.55%
Madi et al. (2005)	Numerical	Multiple	Equant	Deformable	Viscous $n>1$	Mech.	4%
Takeda and Griera (2006)	Numerical	Multiple	Equant	Deformable	Elasto-viscous $n=1$	Flow/mech.	2.5
Groome et al. (2006)	Numerical	Multiple	Equant	Rigid	Viscous $n=1$	Flow/mech.	$\gamma=1.5$
Li et al. (2007)	Physical	Multiple	Equant	Deformable	Spinel–mgo	Mech.	80%
Johnson (2008)	Numerical	Single	Equant	Rigid	Viscous $n\geq 1$	Rotation	$\gamma=1.0$
Groome and Johnson (2008)	Numerical	Multiple	Equant	Rigid	Viscous $n=1$	Mech./flow	$\gamma=1.5$
This study	Numerical	Multiple	Equant	Deformable	Viscous $n\geq 1$	Mech./flow	$\gamma=7.5$

The aim of this work is to systematically study the evolution of a numerical two-phase system to high strains (shear strain between 3 and 7.5) so that the variations in the geometry and flow field can be compared for different combinations of starting materials, viscosity contrasts and stress exponents.

2. Methodology

This study made use of the Elle software (Jessell et al., 2001; Bons et al., 2008; http://www.microstructure.info/elle) to construct a series of numerical experiments using the BASIL non-linear viscous finite element code (Houseman et al., 2008 and references therein).

Elle is a multi-purpose modelling platform designed to simulate the development of microstructures during tectonic and/or metamorphic processes. Elle defines a 2D description of the microstructure, which is described by a contiguous set of polygons (termed "flynns") that are defined by a network of connected boundary nodes (termed "bnodes"). The option to describe the microstructure with unconnected nodes or particles (termed "unodes") was only used in this study to provide passive markers of the deformation field. Properties can be assigned to bnodes and flynns. In this study, rheological properties were assigned to the flynns, where each flynn (representing a single grain) has a homogeneous rheology. Bnodes only served to define the outlines of the flynns. Elle uses both horizontally and vertically wrapping boundaries so that, for example, a flynn that is cut by the right-hand boundary continues on the left side. This means that the model boundary is in fact a unit cell that it is repeated infinitely in all directions. This feature maintains a square model shape and significantly reduces boundary effects.

A single grain aggregate with a foam texture was used to create the initial starting microstructure (Fig. 1). The strength of the hard or soft phase was assigned to each flynn according to the desired fraction of the hard phase. This way an aggregate with approximately 30% and 70% of the hard phase was created. The aggregate with 70% hard phase was created by swapping hard and soft flynns in the 30% model.

The program BASIL is a general-purpose finite deformation calculation package that is adapted to the solution of viscous deformation of a 2D sheet in plane-strain. BASIL is used within Elle to calculate the viscous strain rates and the associated stress field (including pressure) for typical applications that focus on grain-scale processes. However, since BASIL works with dimensionless variables,

the scale of the problem is arbitrary. Internal deformation and material properties, however, are assumed piecewise continuous, i.e., discontinuities are permitted on lines that coincide with element boundaries.

The constitutive law relating the deviatoric stress to the strain rate for incompressible viscous fluid is of the form:

$$\tau = 2\eta\dot{\varepsilon} \tag{1}$$

where η denotes viscosity, which can also be described by:

$$\eta = \left(\frac{B}{2}\right)\dot{E}^{\left(\left(\frac{1}{n}\right)-1\right)} \tag{2}$$

where n is the strain rate exponent, B is the strength coefficient, a material property proportional to the viscosity for materials where $n = 1$, and $\dot{E}$ is the second invariant of the strain rate tensor.

One experimental run consists of the iterative application of small (0.025 γ) increments of dextral simple shear deformation to a model with initially square bounds. Since the BASIL code supports periodic boundary conditions across two of the four sides of the model (in our case the vertical sides), we were able to make use of code within Elle to maintain a constant square boundary at the end of each increment of deformation (see Houseman et al., 2008 for details). Recent modifications to the Elle platform which enable more realistic model evolution are described in Appendix 1.

In these experiments we systematically varied three input parameters (Table 2).

1. The percentage of inclusion grains in the model (ϕ), with approximately 30%, 50% and 70% high or low viscosity inclusions is used here. While the first and last cases represent a configuration in which soft or hard grains are the continuous phases (i.e. matrix), the intermediate case is a transitional configuration in which both phases are locally discontinuous.
2. The viscosity ratio (vr) between grains, with ratios of 1, 5 and 10 is used. It should be noted that for a ratio of vr > 1, the linear and non-linear cases cannot be directly compared, as their effective viscosity ratio is different. These contrasts were used as they show a range of interesting behaviours, above a vr of 10, especially for the $n = 3$ case, there was very little variation.
3. The stress exponent of the non-linearity of the viscosity (n), with either 1 or 3 is used.

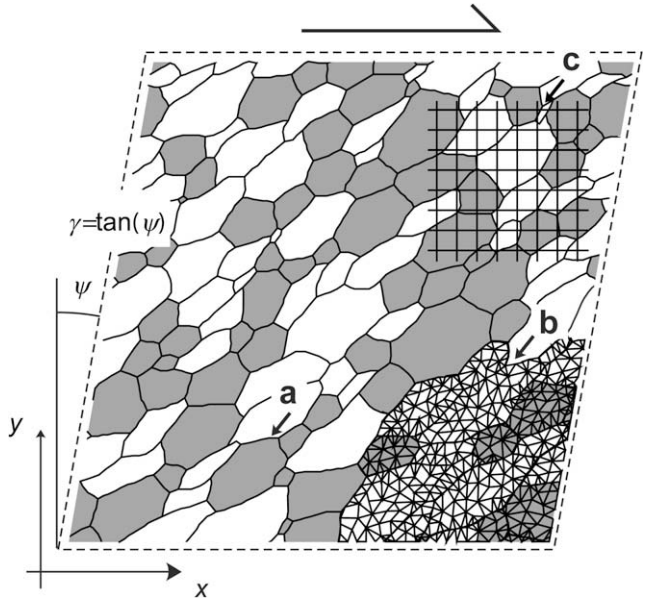

Fig. 1. Example of the initial configuration of the simulations where grey and white colours are, respectively, hard and soft grains. The numerical models consist of three layers (a) a grain boundary network used to define grain boundaries, (b) a Delaunay triangulation mesh adapted to grain boundaries used for FEM calculations at each time step and (c) a passive and initially square grid used to track the local accumulative deformation. Boundary conditions are x and y periodic, with free vertical sides and imposed constant displacement on the horizontal sides of the model.

In all the models, grain boundaries are coherent, and grain viscosities are constant throughout an experiment, i.e. we have not considered strain softening or hardening at the grain scale, although the overall system may exhibit this form of behaviour.

We thus performed 12 distinct experiments, up to a shear strain of 7.5 where possible, although for certain experiments this proved to be impossible (due to non-convergence of the finite element code), and a standard shear strain of 3.0 or 4.0 was recorded.

To confirm the validity and stability of the numerical scheme for single rigid objects, we performed an experiment with a single round rigid object to compare its rotation rate with the theoretical value (see Appendix 1).

3. Results

In order to display the flow behaviour and microstructural evolution of each experiment two complementary techniques were used: grain boundary structures and Lagrangian grids. The starting grain shape and phase distribution microstructures are shown as the first column of Fig. 2a, with white grains having the lower viscosity and grey grains having the higher viscosity in each series. Grain boundaries are shown as black lines, and simply represent passive markers in the system. For this figure we have repeated the microstructure once in the horizontal and vertical directions and this helps to bring out the multigrain structures which extend across large parts of the models. We have subsequently calculated the high strain equivalents of these microstructures for various viscosity ratios (Fig. 2b and c).

We also display the final microstructures overlaying an originally orthogonal, but now passively deformed grid (Fig. 3, here we simply display the model for one unit cell as the detail would be otherwise hard to resolve). The red lines were originally horizontal, and the grey lines vertical.

Showing the complete time evolution of each experiment would result in a vast number of figures, so in this paper we only show the microstructure evolution of one experiment, 10_30_1 (the naming convention for experiments is vr_ϕ_n such that 10_30_1 refers to

Table 2
Experimental setup.

Experiment name	Viscosity ratio vr	% "hard" phase ϕ	Stress exponent n	Timesteps t	Bulk shear strain γ
5_30_1	5	30	1	300	7.5
5_50_1	5	50	1	300	7.5
5_70_1	5	70	1	300	7.5
10_30_1	10	30	1	300	7.5
10_50_1	10	50	1	300	7.5
10_70_1	10	70	1	300	7.5
5_30_3	5	30	3	300	7.5
5_50_3	5	50	3	300	7.5
5_70_3	5	70	3	160	4
10_30_3	10	30	3	160	4
10_50_3	10	50	3	160	4
10_70_3	10	70	3	120	3

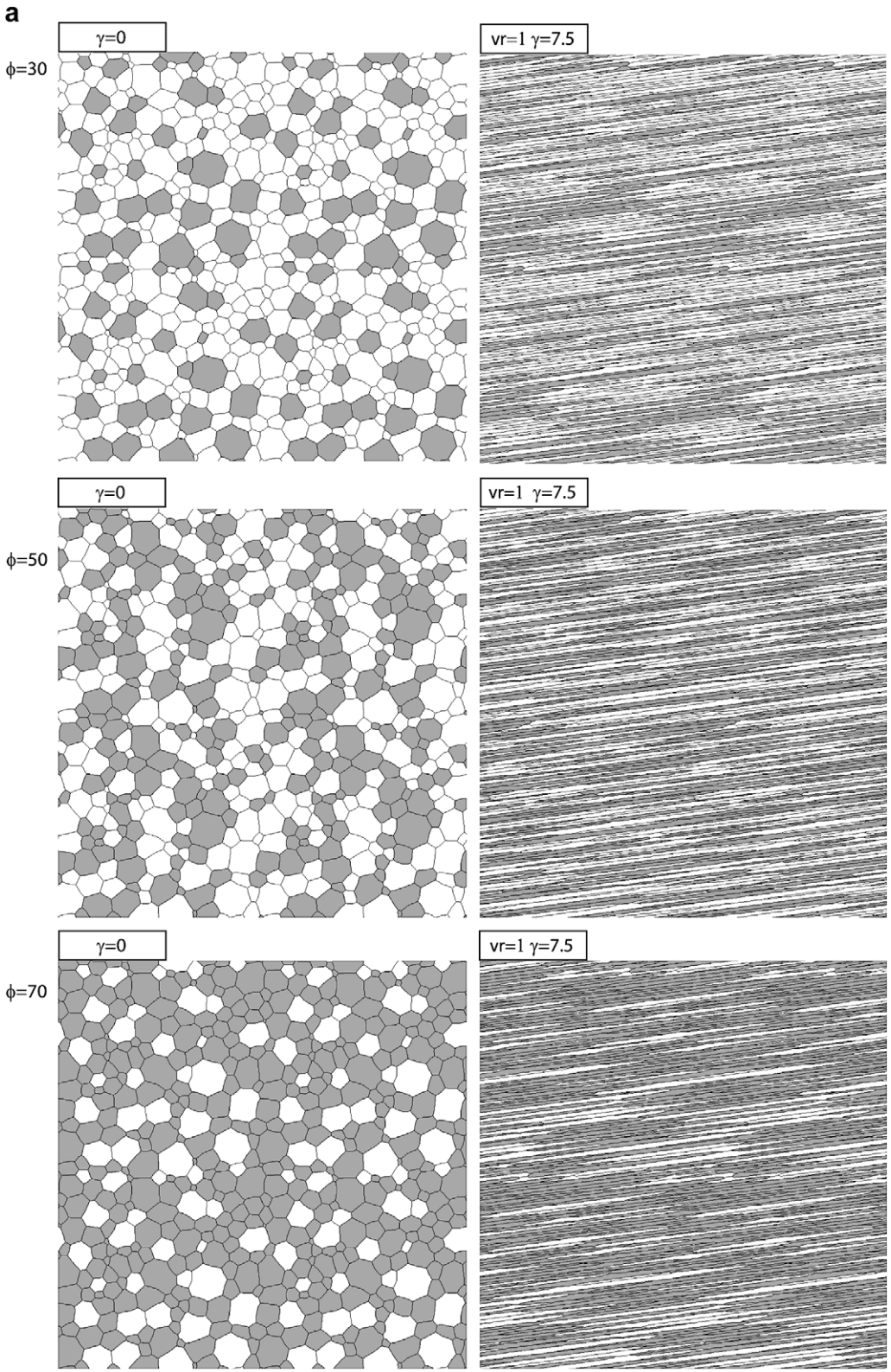

Fig. 2. The systematic variations in final structures of viscous two-phase aggregates to high strain, with each row showing a given percentage fraction of hard grains (ϕ) and varying viscosity ratio (vr), as compared to the starting microstructure. (a) Starting configuration and deformed model for the case of no viscosity contrast. (b) Linear viscous ($n = 1$) behaviour. (c) Non-linear ($n = 3$) behaviour. White grains have the lower viscosity, grey grains the higher viscosity and grain boundaries are marked in black.

vr = 10; $\phi = 30\%$; $n = 1$) as grains and grain boundaries and as a deformed grid (Fig. 4). The reader is invited to consult the online animations to view the other experiments in their entirety (http://tinyurl.com/elleblobs).

3.1. Systematic variations in the final microstructure

Using the homogeneous deformation (vr = 1) as a reference (the second column in Fig. 2a), we can see that in general, the larger the

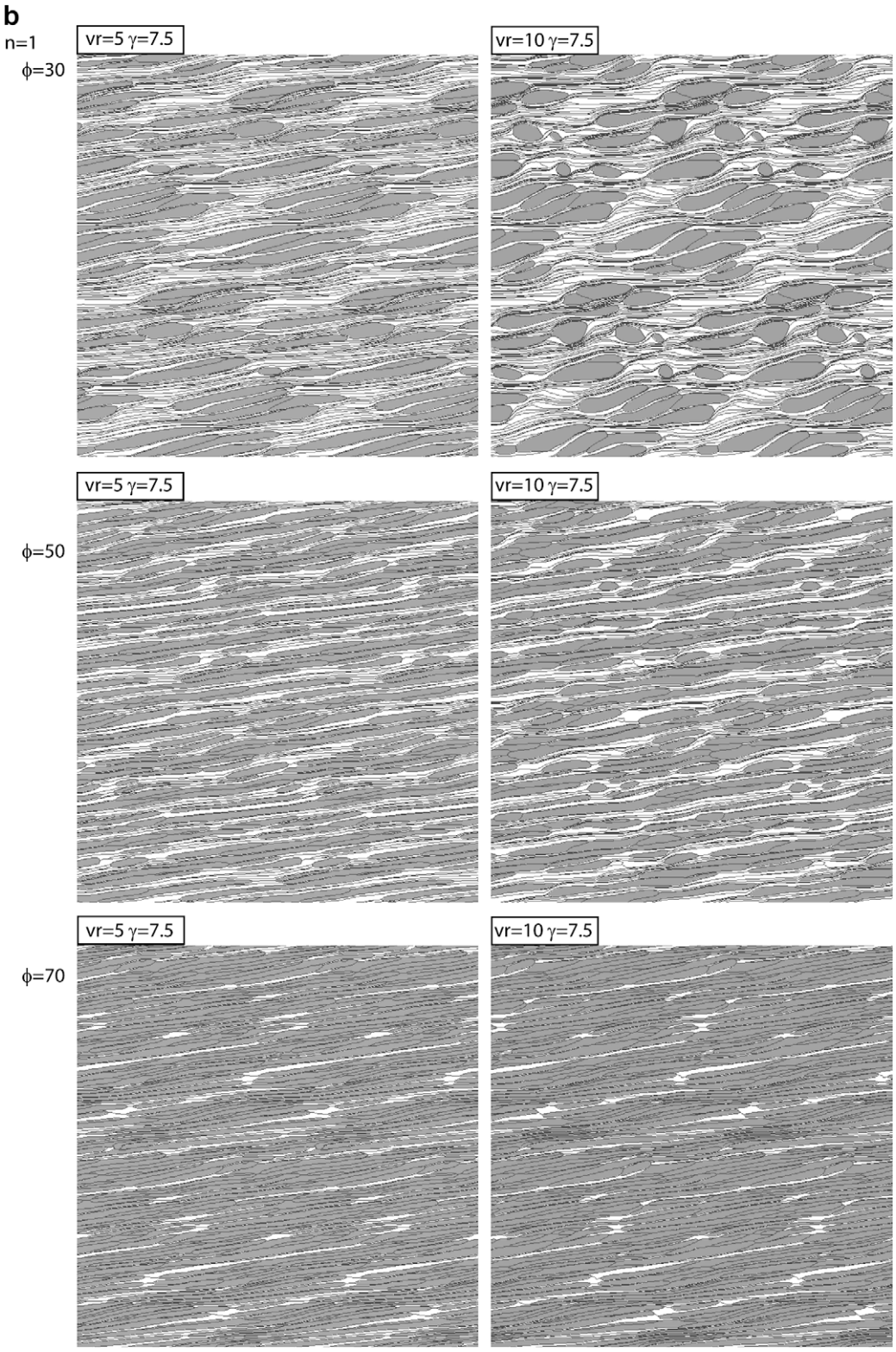

Fig. 2. (*continued*).

viscosity ratio, the larger the *n* value, and the lower the fraction of higher viscous material, the more the deviation from the homogeneous case. The most extreme deviation is thus experiment 10_30_3 (although 10_70_3 localises quite severely as well) and the most similar to homogeneous case is thus 5_70_1. Experiment 10_30_3 is the one that most closely resembles the "rigid objects" commonly discussed in the literature, with zones of localisation in the weaker material wrapping around them. For the rest of this paper we shall use the terms hard and soft to reflect the more and less viscous phases within a single experiment.

The conventional Eshelby (1957) conjecture of an isolated inclusion embedded in a contrasted elastic/viscous medium clearly

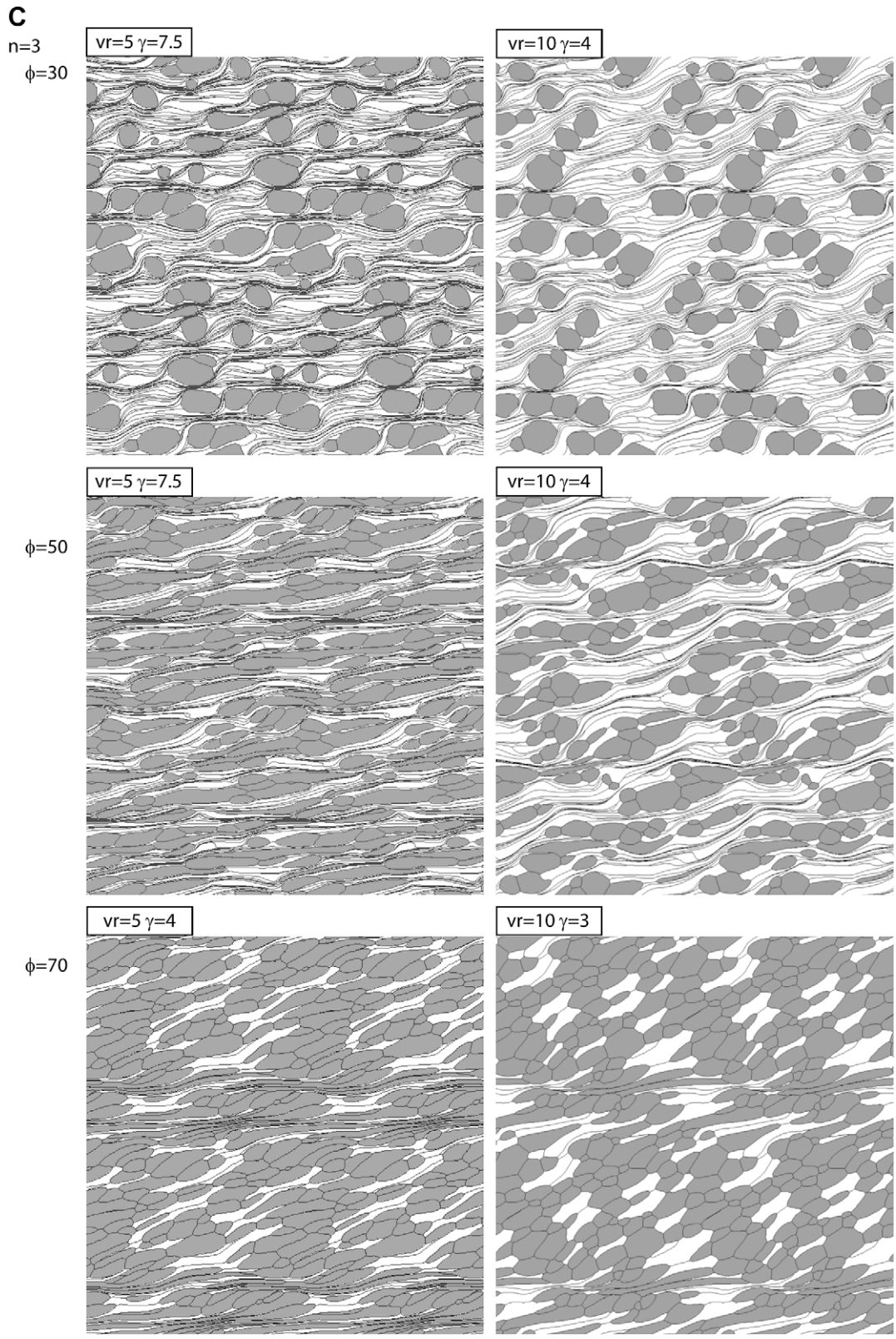

Fig. 2. (*continued*).

cannot be applied here, due to neighbour interactions, and hence we should not be surprised that grains do not deform homogeneously, especially as they did not start with ideal shapes. Second-order approaches will be necessary to estimate macroscopic properties (i.e. bulk stress, strain rate or effective viscosity) of the composite (Lebensohn et al., 2004). Although this effect also can be related to the non-ideal shape of grains or the low resolution of the FEM mesh, similar observations of non-uniform strain field also

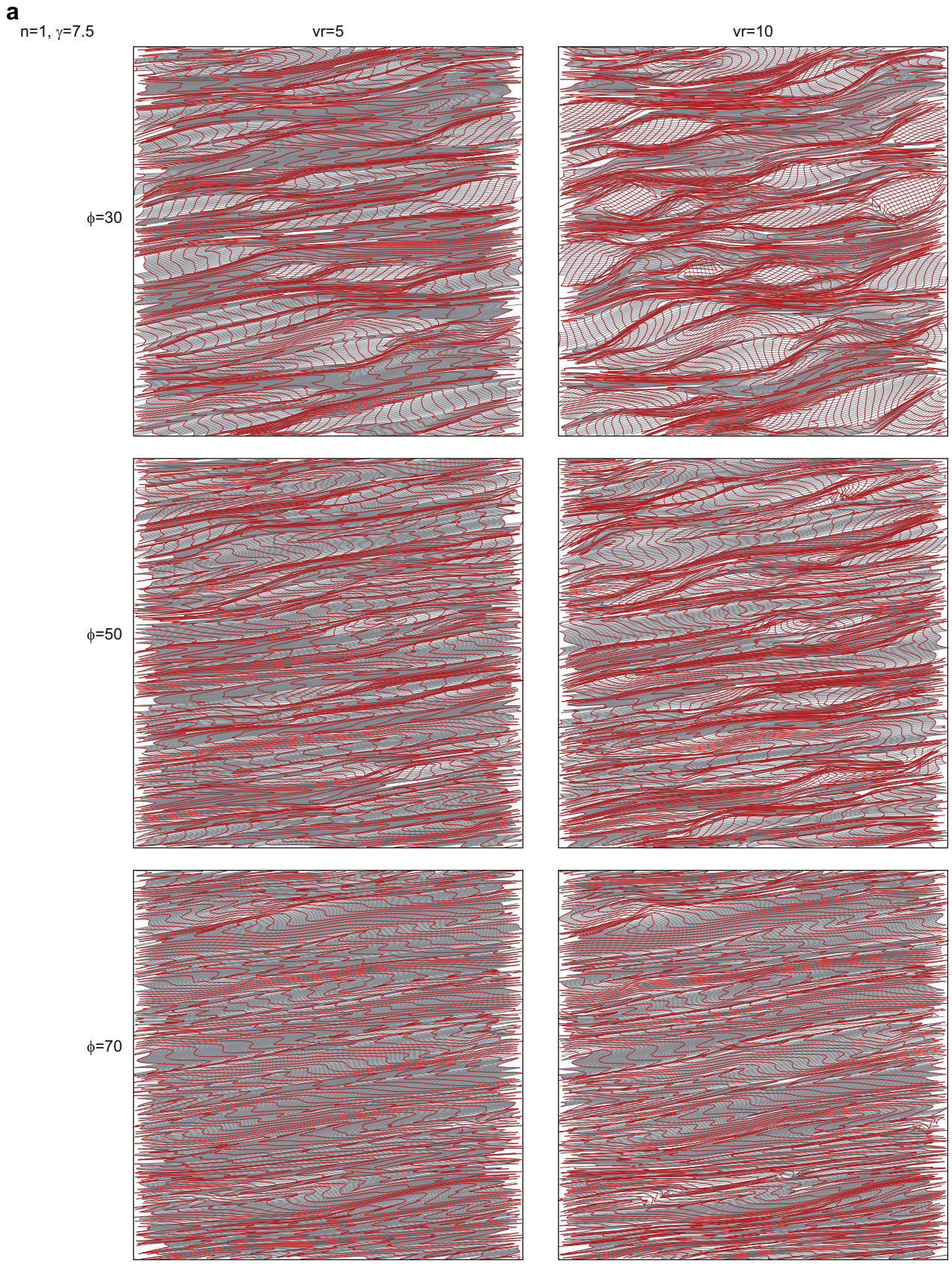

Fig. 3. Finite strain grids for final stages of each vr_ϕ_n combination. (a) Linear viscous ($n = 1$) behaviour. (b) Non-linear ($n = 3$) behaviour. The red lines were initially horizontal, and the grey ones were vertical. Line segments longer than 0.1 of the bounding box are not drawn to reduce the visual confusion, as with high localised strains they overlap significantly.

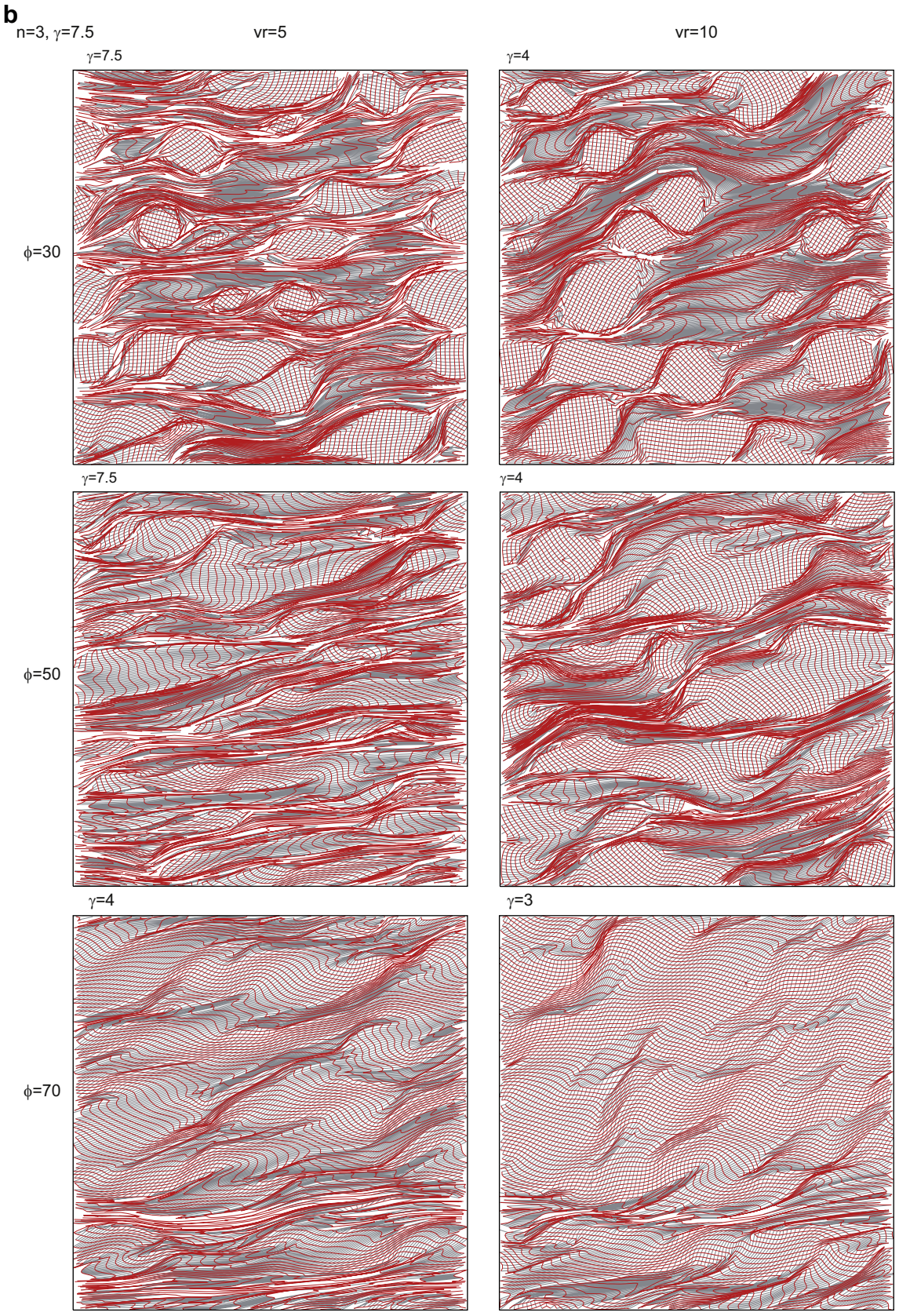

Fig. 3. (*continued*).

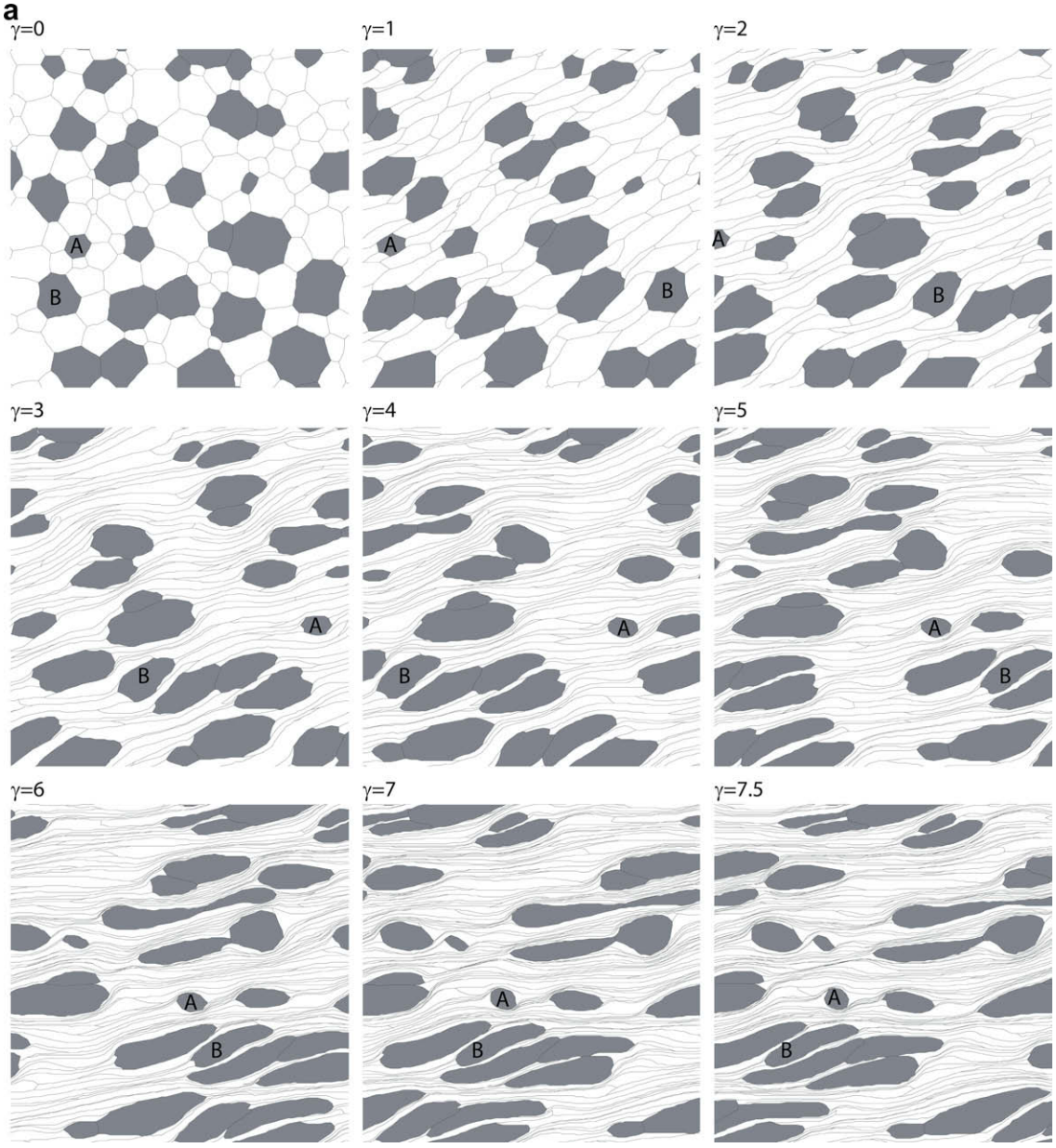

Fig. 4. Sequential evolution of the vr = 10, $\phi = 30\%$, $n = 1$ experiment, up to a shear strain of 7.5. (a) Microstructure evolution. (b) Finite strain grids. (c) Combination of grids and microstructures. The two grains A and B are highlighted for the first three timesteps and their high strain behaviour may be followed to examine the marked contrast in internal deformation between the two grains.

have been reported by Moulinec and Suquet (2003) and interpreted as an evidence of strain localisation.

3.2. Grain shapes

In terms of grain shapes, it is perhaps surprising how much variation there can be within single experiments, with, for example in experiment 10_30_1, axial ratios varying between 1.1 and 9 in the hard phase, which have equal viscosities (Fig. 5). In some cases this reflects an initial elongation due to two hard grains touching; however, in others it reflects the neighbour relations of the hard grains. Those hard grains which are most isolated in the model (e.g. grain A in Fig. 4) from other hard grains are able to rotate in the matrix and thus maintain a relatively round form, as their rotation rate is sufficiently fast that their long axes rotate out of the elongation direction before they become so long that they can no longer rotate. When the hard grains are closely spaced (e.g. grain B in Fig. 4), their rotation is inhibited and they elongate faster than they can rotate, and thus become locked in the extension field.

In the $\phi = 50$ experiments, the notion of grains and matrix is obviously unclear, and the hard and soft grain clusters mechanically act like single grains, and the grain shapes of individual grains in these clusters are not all that meaningful.

3.3. Strain localisation

In these experiments, three types of localisation of deformation can be observed. Localisation at the margins of the hard grains is apparent in many of the runs (Fig. 6a), especially in the $\phi = 30\%$ and 50% series. In the $\phi = 70\%$ $n = 3$ experiments, the soft grains link up to produce strongly localised zones. These two phenomena both fall into the class of *inherited* localisation as defined by Montesi and

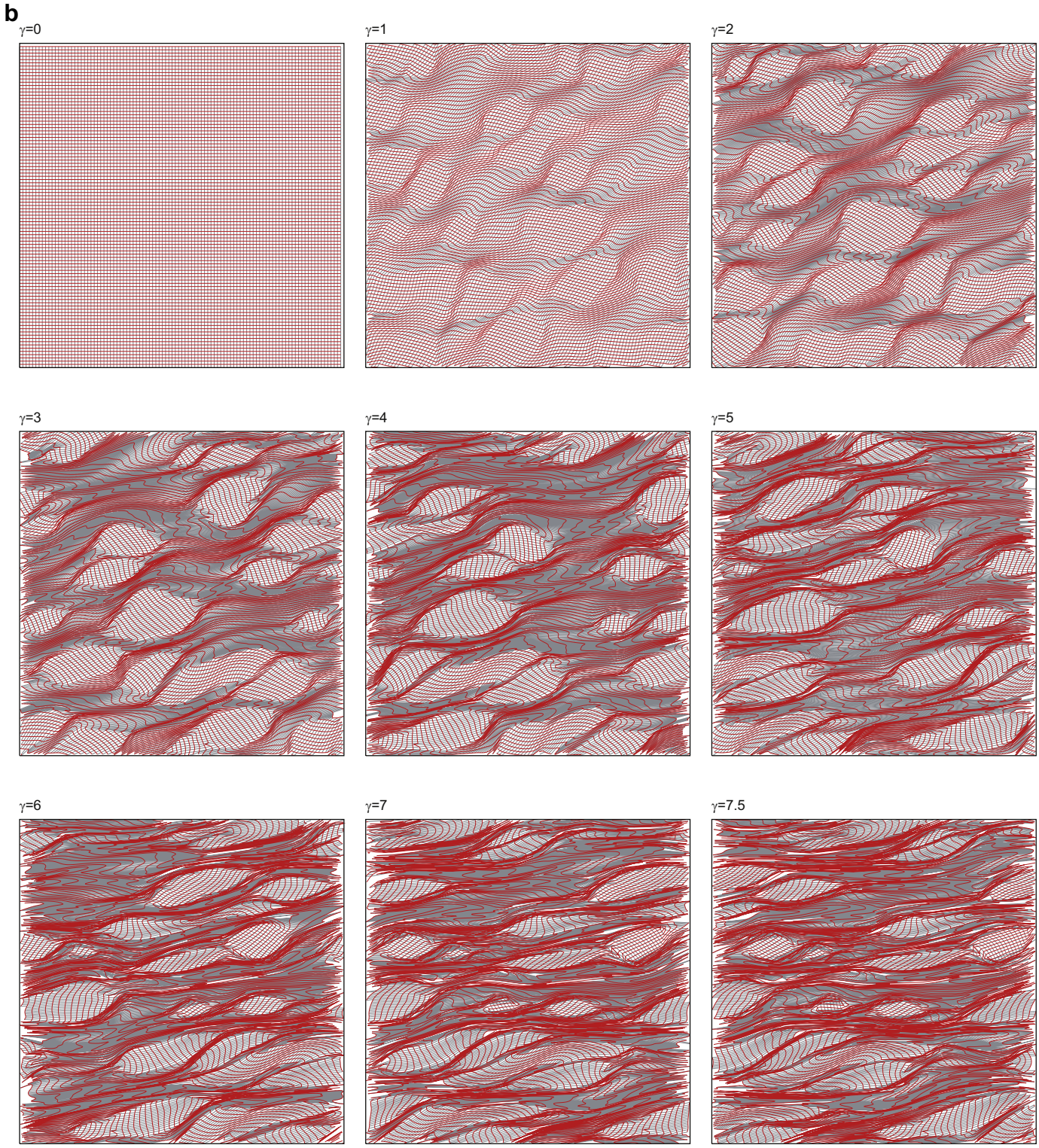

Fig. 4. (*continued*).

Zuber (2002), where the deforming medium is initially heterogeneous and localisation is controlled by the pre-existing structure. When two hard grains pull apart during the deformation, the soft material in-between is forced to stretch, and this leads to a localisation in an otherwise homogeneous material that they call *imposed* localisation, where the boundary conditions are inhomogeneous (Fig. 6b). In some experiments such as 10_30_1, the hard grains rearrange themselves to form horizontal "trains" of grains, with associated zones of soft material on either side. Although there was some clustering of grains in the Y direction at the start of the experiment, the enhancement to produce hard grain free layers, which in simple shear allow the mechanical properties to be dominated by the soft phase, corresponds to a combination of Montesi and Zuber's *inherited* and *dynamic* localisations, the latter

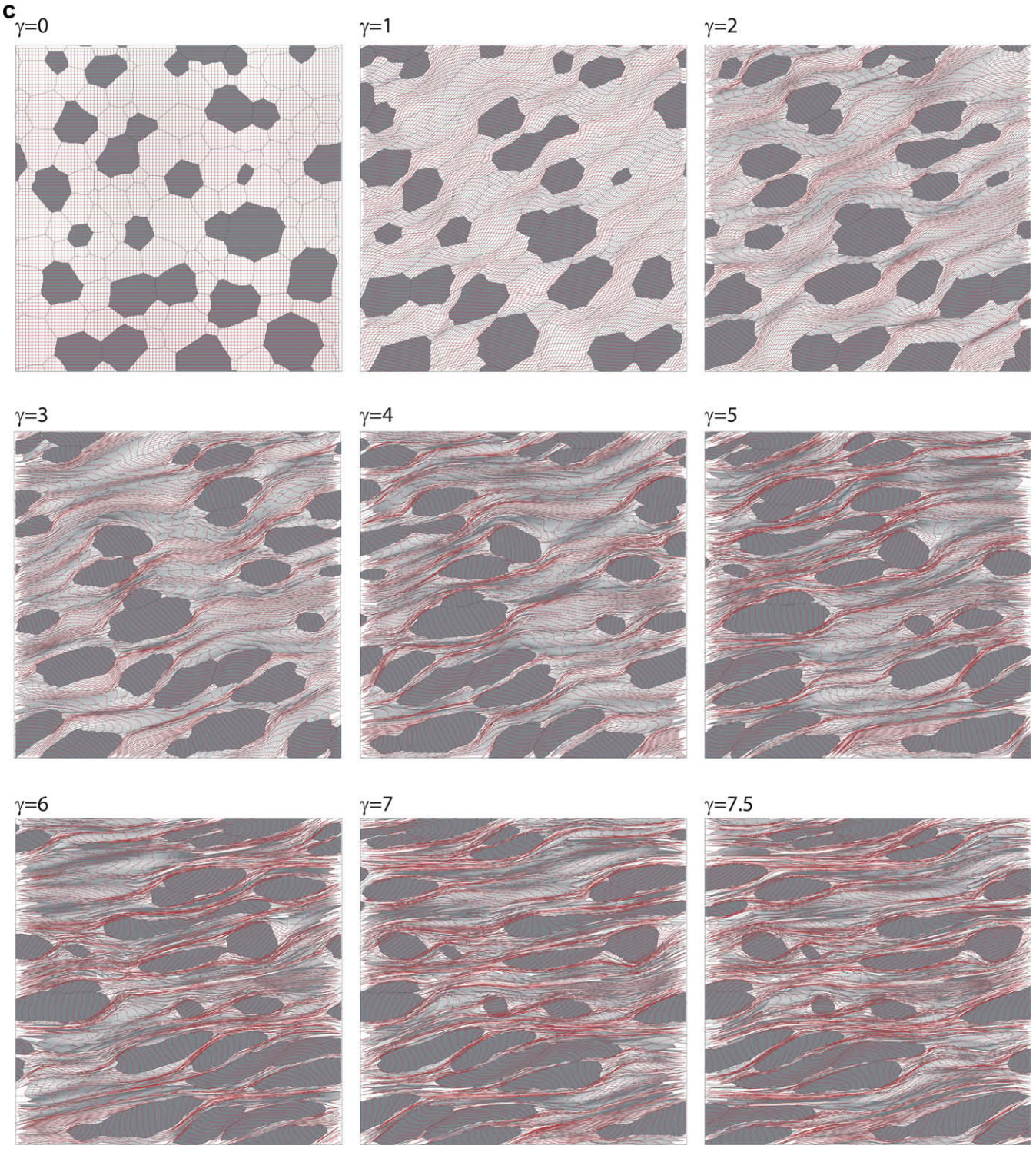

Fig. 4. (*continued*).

occurs when an evolution of material properties during deformation leads to localisation. These aspects bring together different length scales of the strain localisation.

A second type of dynamic localisation is found in the $n=3$ experiments, where individual hard grains show a much more varied finite strain compared to the $n=1$ experiments. In the $\phi=70\%$, $n=3$ experiment an SC-fabric develops (cf. Berthé et al., 1979). Low strain grains define an oblique S-fabric, which is cut by shear plane parallel C-bands, formed by highly strained soft and hard grains. In other experiments (such as 10_30_1 and 10_50_3) C′ structures formed deforming the grain shape S-foliation.

In several experiments (e.g. experiment 5_50_1, Fig. 3b) it is possible to observe perturbation structures associated with hard grains as well developed passive folds develop in the Lagrange mesh. Without this reference grid we would see only the striped elongated grains with small shear bands and thickness variation.

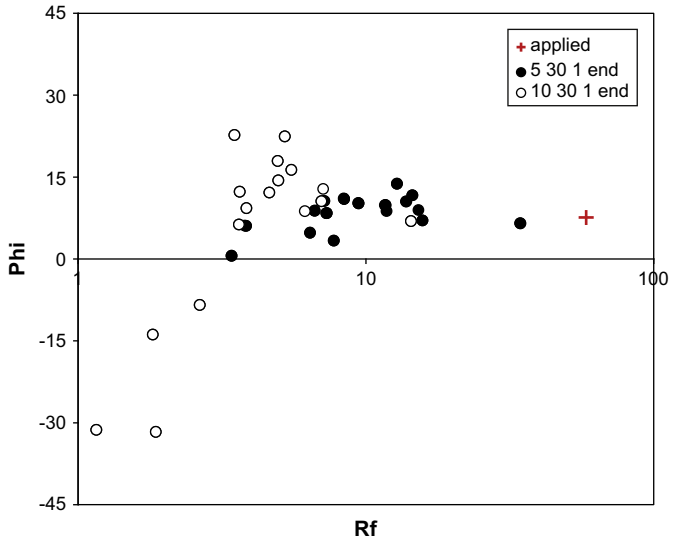

Fig. 5. Graph showing relationship between axial ratio (Rf) and orientation (ϕ) of hard grains from two $n = 1$ experiments, as compared to the orientation and axial ratio of the strain ellipse for $\gamma = 7.5$.

3.4. Millipede structures

Although the hard objects are clearly not meant to simulate porphyroblast behaviour, as they do not grow in size, it is noteworthy that the deformed grid around the isolated grains at the early stages of deformation (e.g. Fig. 7) display a millipede pattern (Bell et al., 1995) even though up until now these have often considered to be evidence for pure shear deformation; as pointed out by Johnson and Bell (1996), this need not be the case. If the hard inclusions were indeed growing porphyroblasts, they would capture the millipede structure as inclusion pattern (Bons et al., 2009).

3.5. Grain rotation

Grain rotation can be best observed by looking at the deformed grids during progressive deformation (such as Figs. 3 and 4b). In these figures, red lines were originally horizontal, and grey lines were vertical. If we examine the intermediate or final orientations, it is striking how many of the grains have rotated the same amount within one experiment at one time, regardless of whether the grains are isolated, in clusters and regardless of whether there has been significant localisation of deformation. If we look at experiment 5_30_3 at a shear strain of 4, for example, we can see that the isolated grains have undergone an average rotation of about 79 degrees, and the two-grain clusters a rotation of 55 degrees (Fig. 8). Looking at either the current red or grey grid orientations, one could be forgiven for thinking that they represented a relict foliation preserved in the hard grains and that the grains themselves had therefore not rotated. There appears to be a slight preference for either grid orientations at a high or low angle to the flow plane, perhaps suggesting an additional reason for this observation in natural systems (Johnson, 1999).

3.6. Non-linear effects

In linear materials the strain rate partitioning between hard and soft phase does not affect the effective viscosity contrast. This is not the case for non-linear situations, in which the effective viscosity contrast will depend on the strain rate ratio between hard and soft

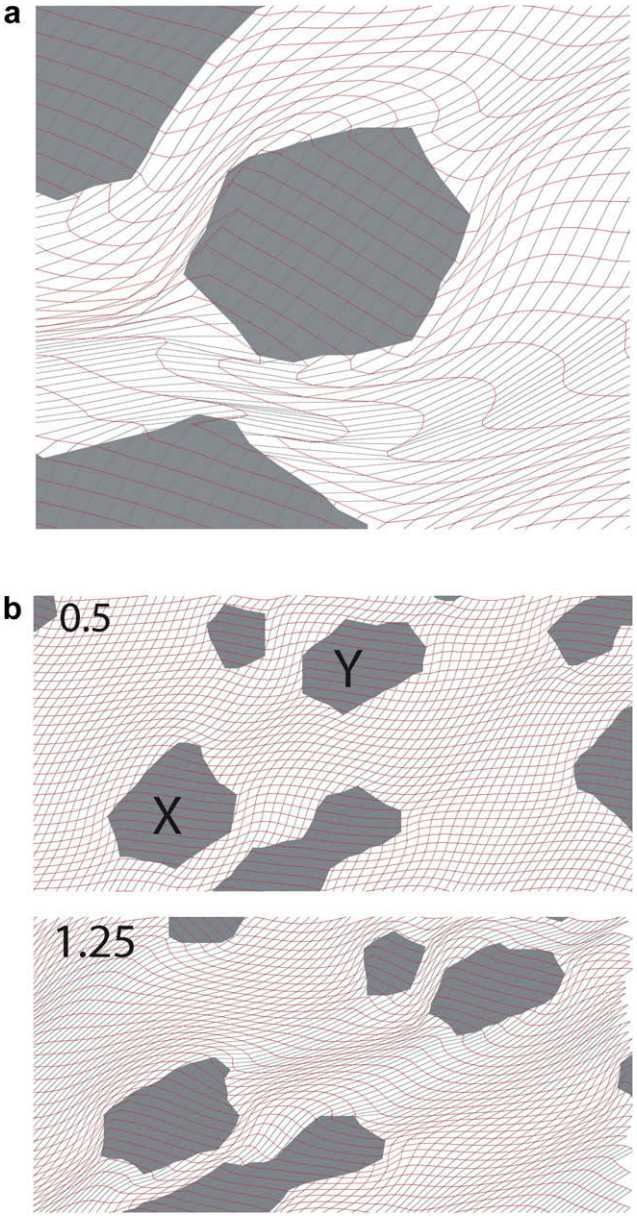

Fig. 6. Types of localisation seen in these experiments. (a) Finite strain grid of a single hard grain from the vr = 5, $\phi = 30\%$, $n = 3$ at a shear strain of 1.25, showing localisation of deformation around the hard grain. (b) Finite strain grid of a two hard grains (X and Y) from the vr = 10, $\phi = 30$, $n = 1$ experiment at a shear strain of 0.5 and 1.25 showing localisation of deformation between the two grains.

phases and their spatial distribution (i.e. if the hard or soft phase is the matrix). Assuming same stress exponent and using the Eq. (2), the effective viscosity ratio can be estimated as

$$\mathrm{vr}_{\mathrm{effective}} - \frac{B_{\mathrm{hard}}\dot{E}_{\mathrm{hard}}^{(1/n-1)}}{B_{\mathrm{soft}}\dot{E}_{\mathrm{soft}}^{(1/n-1)}} = \mathrm{vr}\dot{E}_{\mathrm{p}}^{(1/n-1)} \tag{3}$$

Where vr is the viscosity ratio of reference and $\dot{E}_{\mathrm{p}}$ is the ratio of the second invariant of the strain rate between the hard and soft phases. Experimental results of Bloomfield and Covey-Crump (1993) highlight the importance of the microstructure and spatial distribution of two-phase aggregates to constrain the stress/strain partitioning between phases and the bulk properties of the two-phase aggregate. For a weak-phase supported model, the strain rate

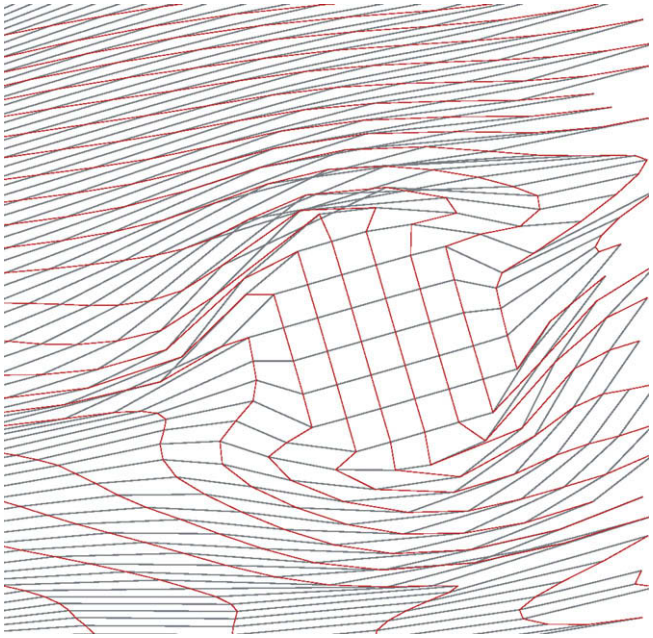

Fig. 7. Grain rotations in the 5_30_3 experiment. Enlargement of a finite deformation grid around a single isolated grain in the experiment vr = 10, $\phi = 30\%$, $n = 3$ at a shear strain of 2.5, showing millipede-like structure to deformed grid. If the grain had been growing to include its surrounding foliation, this could be preserved from further deformation.

ratio can be approximated using the Reuss assumption of uniform stress (Hutchinson, 1976), and then, proportional to the imposed viscosity ratio. The Eq. (3) simplifies to

$$\mathrm{vr}_{\mathrm{effective}} = \mathrm{vr}\left(\frac{1}{\mathrm{vr}}\right)^{(1/n-1)} = \mathrm{vr}^{(2-1/n)} \tag{4}$$

For $n = 3$, the effective viscosity ratios for vr = 5 and vr = 10 are about 15 and 46, respectively. This assumption is valid for microstructures with spherical-shaped hard grains, but the strain rate ratio evolves with increasing deformation due to the increase of the grain's ellipticity and the interactions between neighbouring grains (see Fig. 6a and b of Bloomfield and Covey-Crump, 1993; Takeda and Griera, 2006). Eq. (4) gives an approximation of the effective viscosity contrast for a non-linear medium where the weak-phase is the matrix and allows a comparison with a linear viscous simulation with similar contrast of viscosity. For the opposite situation where the strong-phase is arranged in a continuous framework, the problem can be treated as a load-bearing framework (Tharp, 1983; Handy, 1990) and a first estimation of the strain rate ratio can be found using a uniform strain rate model. However, this assumption generally does not match with observations where a variable strain rate ratio is observed with increase of deformation (Bloomfield and Covey-Crump, 1993; see Fig. 6 of Takeda and Griera, 2006).

Whilst it is tempting to look at the systematic variations in geometries shown in these as representing a possible tool for estimating palaeo-rheology, if we compare a very high viscosity ratio but linear viscous experiment with a lower viscosity ratio but non-linear viscous experiment, the outcomes can be remarkably similar. Fig. 9 shows an example of the similar geometries between non-linear and equivalent linear simulation for 50_30_1 vs. 10_30_3 contrasted by the non-equivalence 50_70_1 vs. 10_70_3 models.

An important result is that strong strain localisation is plausible in models with a high fraction of a hard phase, if the material is non-linear. Mancktelow (2002) suggested that only a small strain localisation is observed in numerical models with non-linear viscous

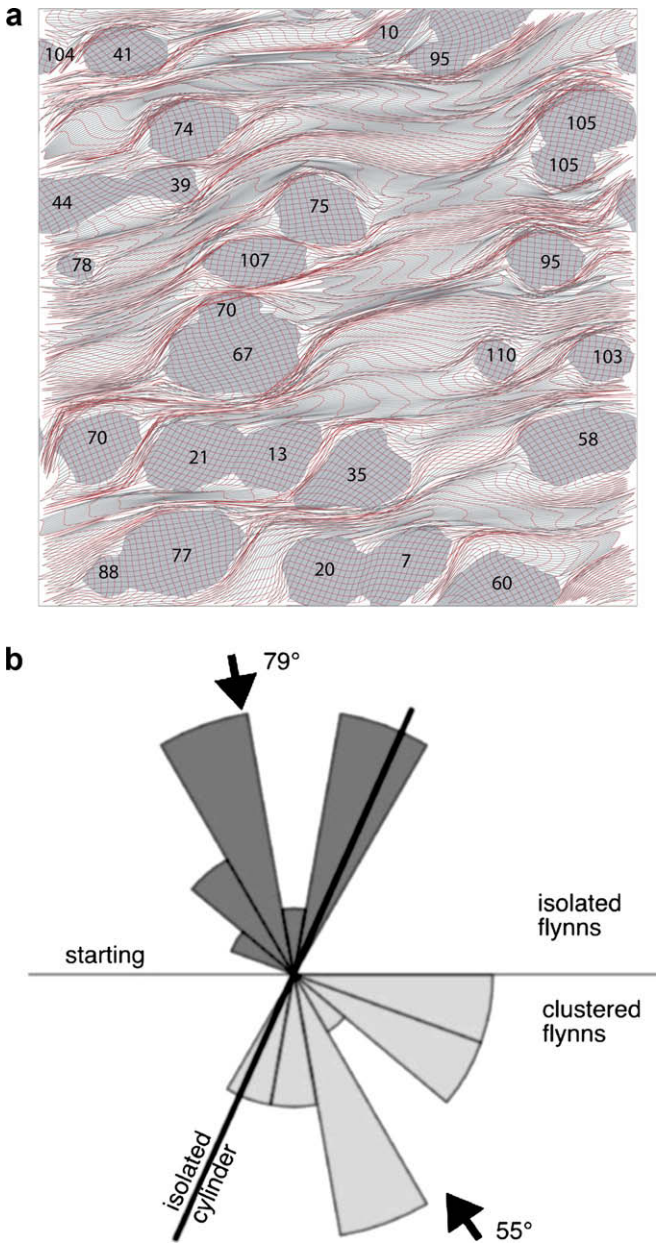

Fig. 8. (a) Combination of finite strain grids and microstructures for an experiment with vr = 10, $\phi = 30\%$, $n = 1$ at a shear strain of 4. The numbers show the average rotation of the red grid lines from the horizontal for each grain. The single grains show a higher average rotation (about 80 degree) than the grain clusters (55 degree). (b) Rose diagram representing the rotations of initially horizontal passive lines in hard grains in the 5_30_3 experiment. Isolated grains (top) rotate more (79 degree) than grains that form part of clusters where two or more inclusions share grain boundaries (bottom, 55 degree). Some of the hard grains rotated as much as an isolated rigid circular grain in an infinite soft matrix would theoretically rotate (115 degree).

behaviour, and advocate additional strain softening effects to explain natural strain localisation in natural rocks. This is consistent with our simulations for linear viscous rheologies. However, non-linear behaviour shows strong strain partitioning between low and high strain regions. The low strain regions show preserved/development of shape preferred orientation (low strain) while shear band localisation and ribbon/layered geometries develop in high strain regions. One of the principal differences with the experimental setup described by Mancktelow (2002) is the ratio of object size to spacing (approximately 1:5 in his experiments, 1:2 here). Another major difference is that Mancktelow only went to gamma of 1. For

higher vr, changes in the spatial distribution of the hard grains usually happen after that.

The difference in results warrants further investigation to see where the difference lies: in the differences in boundary conditions between the two models, in the finite strain, in the material properties or in the starting geometries.

4. Discussion and conclusions

The experiments described in this paper of course ignore a large number of factors that in natural systems will complicate matters. Their utility is precisely that they provide a "baseline" for interpretation of more complex situations: such as more complex or evolving rheologies (e.g. Jessell et al., 2005); non-continuum processes (e.g. Ford et al., 2002; Ford and Wheeler, 2004); or more complex loading histories. This allows us to suggest, for example, that intense localisation of deformation in the softer matrix of the two-phase material can be an *imposed* localisation in the sense of Montesi and Zuber (2002), without recourse to complex rheologies.

The experiments with $\phi = 30\%$ confirm that strain is localised in the soft phase when that phase forms a connected matrix or load-bearing framework (Handy, 1994). In that case, close to the Reuss bound, stress is approximately homogeneous and strain rate highly

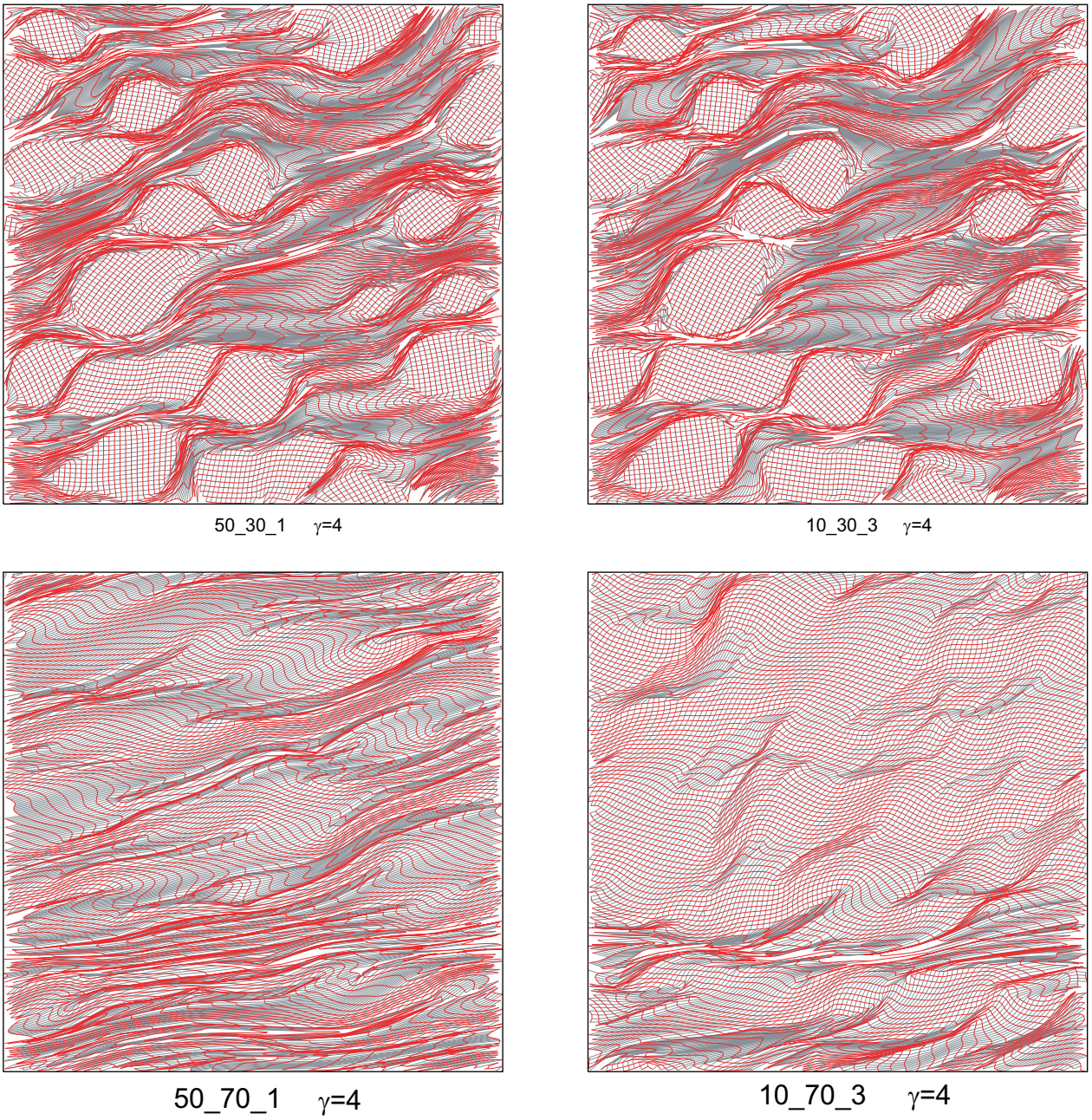

Fig. 9. A comparison between the calculated finite strain grids for two high viscosity ratio, but linear viscous experiments and two low viscosity ratio, but non-linear viscous experiments. In the case of the 50_30_1 and 10_30_3 the grids display almost identical patterns, whereas for the 50_70_1 vs. 10_70_3 experiments the localisation is significantly more developed in the $n = 3$ experiment.

variable, with the soft matrix able to flow around the hard phase. It is observed that an increase in viscosity ratio and an increase in stress exponent generally have the same effect on the microstructure. This means it is difficult to use a system with hard inclusions in a soft matrix as a palaeo-rheology gauge. Above a certain viscosity ratio, isolated hard grains and clusters essentially behave as rigid objects. At $n = 1$ this ratio is between 10 and 50, while at $n = 3$, vr = 10 already makes the hard objects effectively rigid. There is no matrix and disperse phase at $\phi = 50\%$. However, the situation remains close to the $\phi = 30\%$ case, as the soft phase still percolates across the sample in one (initially vertical) direction. This means that the soft phase can still take up most of the strain.

Microstructural evolution is quite different at $\phi = 70\%$, where the hard phase forms the load-bearing framework. The dispersed soft phase grains are constrained in their deformation and cannot take up most of the strain. Mechanically, the aggregate is close to the Voigt or Taylor bound, with strain rate relatively homogeneous and stress relatively variable. Highest stresses occur where the hard phase framework is the sparsest, i.e. where it forms bridges between soft grains, which is in the lower part of the model. With $n = 1$ this is hardly noticeable, as the increase in strain rate in the more stressed grains is proportional to the increase in stress. However, the microstructure is significantly different when $n = 3$. The increase in stress in the stressed grains is raised to the power three for their strain rate, resulting in some hard grains shearing much more than others. The result is the formation of an SC-fabric as defined by Berthé et al. (1979). The C-bands are formed by localised shearing in zones with a relatively high proportion of the soft phase, combined with an increased strain rate of the hard grains in these zones. With the C-bands taking up most of the strain, the remaining material experiences much less strain and develops an oblique grain shape, or S-foliation.

SC-fabrics are most common in sheared granitoids, where the feldspars form the dominant, hard phase. The $\phi = 70\%$ experiment is therefore most comparable to a deforming granitoid.

Fig. 10a shows a strongly sheared pegmatite from Cap de Creus (Druguet et al., 1997) with a distinct SC-fabric. This fabric strongly resembles the $\phi = 70\%$ $n = 3$ case, suggesting that the material was non-linear in its rheology. However, such "ideal" SC-fabrics are not common in the pegmatites at Cap de Creus. In most cases, the sheared pegmatites resemble the $\phi = 50$ experiments (Fig. 10b). This is probably due to diminution of feldspar at the rims of grains, where the resulting fine quartz–feldspar mix becomes part of the soft matrix, which then quickly forms the load-bearing framework. This aspect was not included in the modelling.

The wide range of apparent strains (as defined by axial ratios) for the same viscosities, and roughly equant starting geometries suggest that care needs to be taken when using these microstructures when the modal percent of the rigid phase is high.

If we refer to the "theoretical" literature (analytical, physical and numerical experiments, as opposed to field interpretation), in terms of strain state, starting configuration and mechanical properties, the experiments described here most closely relate to those of Burg and Wilson (1987), Bloomfield and Covey-Crump (1993), Bons and Urai (1996), Dell'Angelo and Tullis (1996) and Takeda and Griera (2006). The experiments described here support the results of Dell'Angelo and Tullis and Takeda and Griera who show that when the dispersed phase (low temperature quartz in the case of Dell'Angelo and Tullis) is weaker or similar in strength to the matrix phase (feldspar), the matrix phase is able to deform homogeneously, and the phase

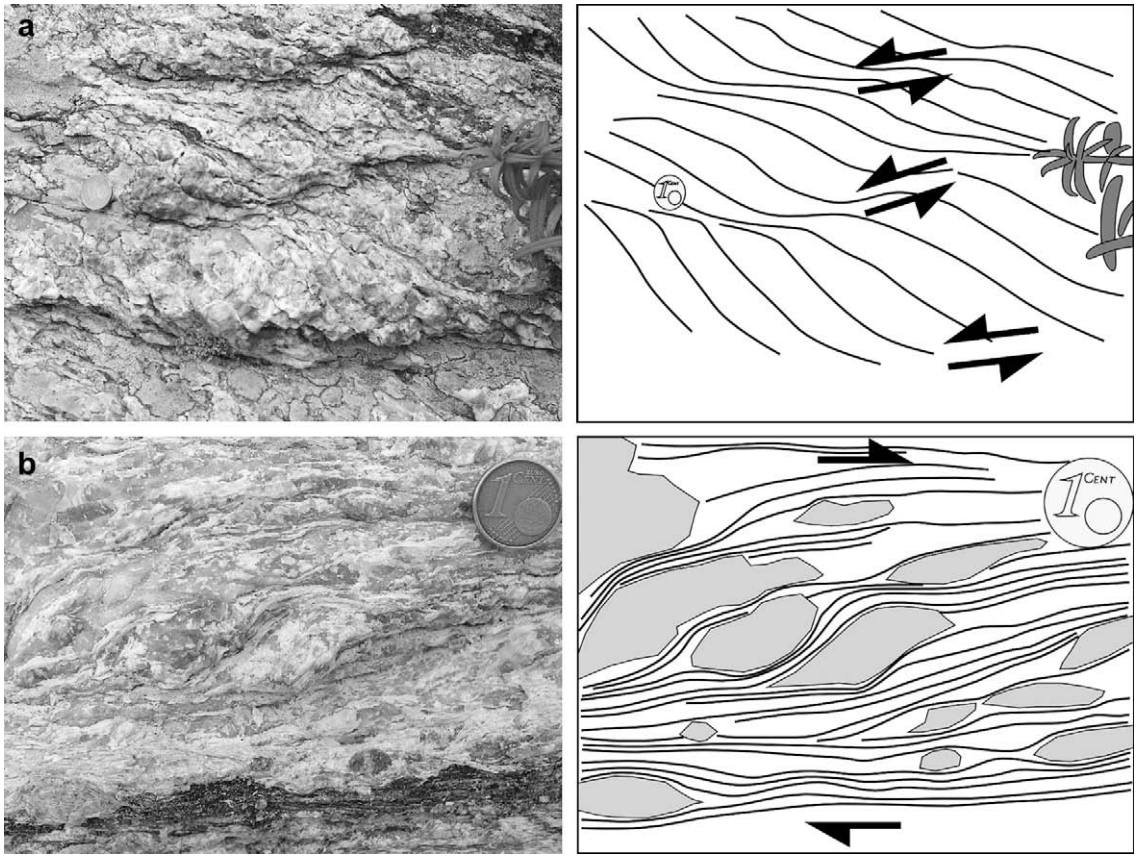

Fig. 10. Sheared pegmatites at Cap de Creus, NE Spain. (a) SC-fabric that strongly resembles the $\phi = 70\%$ $n = 3$ case. (b) Train of feldspar grains (grey) surrounded by matrix of quartz and fine-grained feldspar (white). Diameter of 1 €cent coin for scale is 16 mm.

distribution does not change significantly even at moderately high strains. In contrast when the dispersed phase is significantly stronger than the matrix phase, the matrix phase deforms inhomogeneously, and increased strain localisation causes increased connectivity of the weaker phase.

The finite rotation of the isolated harder objects in the $\phi = 30\%$ experiments was found to be quite similar regardless of the viscosity contrast. Although the small number of objects in each experiment means that we cannot give detailed statistics, and further work repeating these experiments for different starting configurations would be needed, there is at least the suggestion that the complexity of the flow field for such multi-object systems is insufficient to completely disturb the underlying 'single-object' behaviour, so that on average they have similar rotation rates.

Finally, although these experiments have been framed in terms of grain-scale observations, the mechanical and geometric evolution of the system could equally well be applied to scales up to a few hundred metres, although the starting geometries might be harder to justify.

Acknowledgements

University of Touluose III Poste Rouge and DFG ESF EUROCORES Euromінsci support to PDB; CNRS ESF EUROCORES Eurominsci support to AG; and Australian Research Council support for CJLW and LAE. We would like to thank Scott Johnson and Sue Treagus for their thoughtful reviews.

Appendix 1. Modelling characteristics

Boundary conditions

In previous BASIL experiments of this type (Bons et al., 1997; Johnson, 2008; Groome and Johnson, 2008; Jessell et al., 2005) the vertical boundaries were periodic, whereas the horizontal boundaries were fixed so that the positions of material points on the horizontal boundaries were specified by the displacement conditions. In these experiments we developed an additional algorithm that effectively frees up the horizontal boundaries as well. Prior to each increment of deformation, the model is displaced in the vertical direction by an arbitrary amount, the model is then deformed, and the inverse vertical displacement is then applied to the model. In this way although for any one time step the same fixed displacement boundary conditions are applied to the model, the exact placement of the fixed boundary varies randomly for each time step, so that after 300 timesteps, 300 different randomly assigned horizontal levels were held fixed. Therefore, our models effectively have periodic mechanical conditions in both the X and Y directions.

Mesh adjustment and disaggregation

In typical Lagrangian finite element codes, the mesh defines the limits of material properties, and this mesh deforms as the material deforms. When used within the Elle platform, BASIL uses grain boundary polygons to limit material properties, and the mesh is calculated from scratch at each time step. Since viscous rheologies do not exhibit memory effects, the mesh update routine does not need to interpolate the stress and strain rate tensors that would be required in elastic/plastic based materials. In addition we allow a small increment of grain boundary migration (Bons et al., 2008) per time step, which has the effect of increasing triple junction angles, which makes the finite element meshes more stable as the grains become increasingly flattened due to deformation. A favourable by-product of this process is that it allows two adjacent grains that become severely elongated to actually separate, resulting in a local change in the topology of the microstructure (Fig. A1)

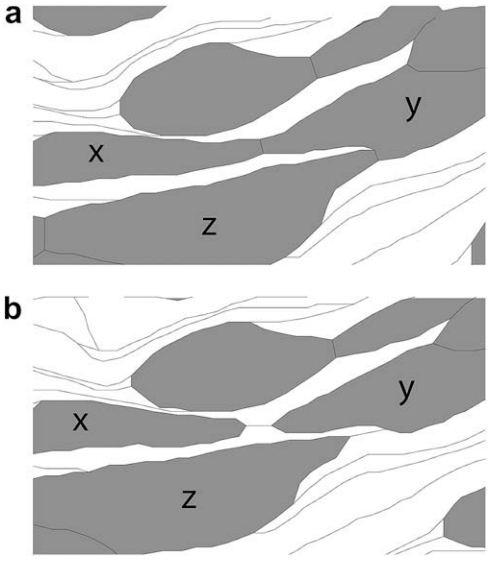

Fig. A1. Disaggregation of previously adjacent grains resulting in implementation of grain growth algorithm during the experiment vr = 5, $\phi = 50\%$, $n = 3$ at a shear strain of 3. (a) Three touching grains at a shear strain of 3. (b) The same three grains, after an additional shear strain of 0.5, are not longer in contact, and thus the stress linkage between the grains is lost.

Benchmark

The numerical prediction for the rotation of a "rigid" circular inclusion (vr = 100, 1000) in a soft matrix has been compared with Jeffery's (1922) theoretical solution (Fig. A2). The comparison shows that the numerical results fit with the analytical solution and the continuous updating of the mesh does not generate divergence of the orientation and rotation rate of the inclusion. Additionally, values of stress and strain rate inside the inclusion are in agreement (but not shown here) with the analytical solution obtained by Schmid and Podladchikov (2004).

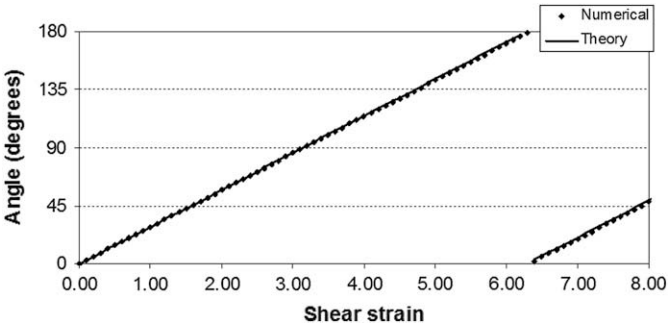

Fig. A2. Comparison of numerical results with the analytical solution for the orientation of an originally horizontal line inscribed on a rigid circular inclusion (vr = 1000, $n = 1$).

References

Bell, T.H., Forde, A., Wang, J., 1995. A new indicator of movement direction during orogenesis: measurement technique and application to the Alps. Terra Nova 7, 500–508.

Berthé, D., Choukroune, P., Jegouzo, P., 1979. Orthogneiss, mylonite and non-coaxial deformation of granites: the example of the South Armorica Shear Zone. Journal of Structural Geology 1, 31–42.
Bilby, B.A., Eshelby, J.D., Kundu, A.K., 1975. The change of shape of a viscous ellipsoidal region embedded in a slowly deforming matrix having a different viscosity. Tectonophysics 28, 265–274.
Bloomfield, J.P., Covey-Crump, S.J., 1993. Correlating mechanical data with microstructural observations. Journal of Structural Geology 15, 1007–1019.
Bons, P.D., Urai, J.L., 1994. Experimental deformation of two-phase rock analogues. Materials Science and Engineering A175, 221–229.
Bons, P.D., Cox, J.D., 1994. Analogue experiments and numerical modelling on the relation between microgeometry and flow properties of polyphase materials. Materials Science and Engineering A175, 237–245.
Bons, P.D., Urai, J.L., 1996. An apparatus to experimentally model the dynamics of ductile shear zones. Tectonophysics 256, 145–164.
Bons, P.D., Barr, T.D., ten Brink, C.E., 1997. The development of δ-clasts in non-linear viscous materials: a numerical approach. Tectonophysics 270, 29–41.
Bons, P.D., Jessell, M.W., Griera, M.W., 2009. Comment to Fay et al. (2008) porpyroblast rotation versus nonrotation: conflict resolution!. Geology 37, e182–e188. doi:10.1130/G25131C.1.
Bons, P.D., Koehn, D., Jessell, M.W. (Eds.), 2008. Microdynamics Modelling. Lecture Notes in Earth Sciences, vol. 106. Springer, Berlin, p. 405.
Bruhn, D.F., Olgaard, D.L., Dell'Angelo, L.N., 1999. Evidence for enhanced d formation in two-phase rocks: experiments on the rheology of calcite-anhydrite. Journal of Geophysical Research 104, 707–724.
Burg, J.P., Wilson, C.J.L., 1987. Deformation of two phase systems with contrasting rheology. Tectonophysics 135, 199–205.
Ceriani, S., Mancktelow, N.S., Pennacchioni, G., 2003. Analogue modelling of the influence of shape and particle/matrix interface lubrication on the rotational behaviour of rigid particles in simple shear. Journal of Structural Geology 25, 2005–2021.
Dell'Angelo, L.N., Tullis, J., 1996. Textural and mechanical evolution with progressive strain in experimentally deformed aplite. Tectonophysics 256, 57–82.
Dresen, G., Evans, B., Olgaard, D., 1998. Effect of quartz inclusions on plastic flow in marble. Geophysical Research Letters 25, 1245–1248.
Druguet, E., Passchier, C.W., Carreras, J., Victor, P., den Brok, S., 1997. Analysis of a complex high-strain zone at Cap de Creus, Spain. Tectonophysics 280, 31–45.
Eshelby, J.D., 1957. The determination of the elastic field of an ellipsoidal inclusion, and related problems. Journal of Fluid Mechanics 67, 376–396.
Ferguson, C.C., 1979. Rotations of elongate rigid particles in slow non-Newtonian flows. Tectonophysics 60, 247–262.
Ford, J.M., Wheeler, J., 2004. Modelling interface diffusion creep in two-phase materials. Acta Materialia 52, 2365–2376.
Ford, J.M., Wheeler, J., Movchan, A.B., 2002. Computer simulation of grainboundary creep. Acta Materialia 50, 3941–3955.
Gay, N.C., 1968. Pure shear and simple shear deformation of inhomogeneous vicous fluids. 1. Theory. Tectonophysics 5, 211–234.
Ghosh, S.K., Ramberg, H., 1976. Reorientation of inclusions by combination of pure shear and simple shear. Tectonophysics 34, 1–70.
Groome, W.G., Johnson, S.E., 2008. Transient strain-rate partitioning during porphyroblast growth. In: Bons, P.D., Koehn, D., Jessell, M.W. (Eds.), Microdynamics Simulation. Lecture Notes in Earth Sciences, vol. 106. Springer, Berlin, p. 405.
Groome, W.G., Johnson, S.E., Koons, P.O., 2006. The effects of porphyroblast growth on the effective viscosity of metapelitic rocks: implications for the strength of the middle crust. Journal of Metamorphic Geology 24, 389–407.
Handy, M.R., 1990. The solid-state flow of polymineralic rocks. Journal of Geophysical Research 95, 8647–8661 (Corrected version: Journal of Geophysical Research, 97, 1897–1899).
Handy, M.R., 1994. Flow laws for rocks containing two non-linear viscous phases: a phenomenological approach (the corrected form). Journal of Structural Geology 16, 287–301.
Houseman, G., Barr, T., Evans, L., 2008. Basil: stress and deformation in a viscous material. In: Bons, P.D., Koehn, D., Jessell, M.W. (Eds.), Microdynamics Simulation. Lecture Notes in Earth Sciences, vol. 106. Springer, Berlin, p. 405.
Hutchinson, J.W., 1976. Bounds and self-consistent estimates for creep of polycrystalline materials. Proceedings of the Royal Society of London Series A 348, 101–127.
Ildefonse, B., Mancktelow, N.S., 1993. Deformation around rigid particle: influence of slip at the particle/matrix interface. Tectonophysics 221, 345–359.
Ildefonse, B., Launeau, P., Bouchez, J.L., Fernandez, A., 1992. Effect of mechanical interactions on the development of shape preferred orientations: a two-dimensional experimental approach. Journal of Structural Geology 14, 73–83.
Jeffery, G.B., 1922. The motion of ellipsoidal particles immersed in a viscous fluid. Proceedings of the Royal Society of London Series A 102, 161–179.
Jessell, M.W., Bons, P.D., Evans, L., Barr, T., Stüwe, K., 2001. Elle: a micro-process approach to the simulation of microstructures. Computers and Geosciences 27, 17–30.
Jessell, M.W., Siebert, E., Bons, P.D., Evans, L., Piazolo, S., 2005. A new type of numerical experiment on the spatial and temporal patterns of localization of deformation in a material with a coupling of grain-size and rheology. Earth and Planetary Science Letters 239, 309–326.
Ji, S.C., Wang, Q., Xia, B., Marcotte, D., 2004. Mechanical properties of multiphase materials and rocks: a phenomenological approach using generalized means. Journal of Structural Geology 26, 1377–1390.
Johnson, S.E., 1999. Near-orthogonal foliation development in orogens: meaningless complexity, or reflection of fundamental dynamic processes? Journal of Structural Geology 21, 1183–1187.
Johnson, S.E., 2008. Strain localisation and rigid-object kinematics. In: Bons, P.D., Koehn, D., Jessell, M.W. (Eds.), Microdynamics Simulation. Lecture Notes in Earth Sciences, vol. 106. Springer, Berlin, p. 405.
Johnson, S.E., Bell, T.H., 1996. How useful are 'millipede' and other similar porphyroblast microstructures for determining synmetamorphic deformation histories? Journal of Metamorphic Geology 14, 15–28.
Johnson, S.E., Vernon, R.H., Upton, P., 2004. Foliation development and progressive strain rate partitioning in the crystallizing carapace of a tonalite pluton: microstructural evidence and numerical modeling. Journal of Structural Geology 26, 1845–1865.
Jordan, P.G., 1987. The deformational behaviour of bimineralic limestone-halite aggregates. Tectonophysics 135, 185–197.
Lebensohn, R.A., Liu, Y., Ponte Castañeda, P., 2004. Macroscopic properties and field fluctuations in model power-law polycrystals: full-field solutions versus self-consistent estimates. Proceedings of Royal Society of London, Series A 460, 1381–1405.
Li, L., Addad, A., Weidner, D., Long, H., Chen, J., 2007. High pressure deformation in two-phase aggregates. Tectonophysics 439, 107–117.
Liu, K.M., McVeigh, C., 2008. Predictive multiscale theory for design of heterogeneous materials. Computational Mechanics 42, 147–170.
Madi, K., Forest, S., Cordier, P., Boussuge, M., 2005. Numerical study of creep in two-phase aggregates with a large rheology contrast: implications for the lower mantle. Earth and Planetary Science Letters 237, 223–238.
Mancktelow, N.S., 2002. Finite-element modelling of shear zone development in viscoelastic materials and its implication for localisation of partial melting. Journal of Structural Geology 24, 1045–1053.
Mancktelow, N.S., Arbaret, L., Pennacchioni, G., 2002. Experimental observations on the effect of interface slip on rotation and stabilization of rigid particles in simple shear and a comparison with natural mylonites. Journal of Structural Geology 24, 567–585.
Mandal, N., Samanta, S.K., Chakraborty, C., 2001. Numerical modelling of heterogeneous flow fields around rigid objects with special reference to particle paths, strain shadows and foliation drag. Tectonophysics 330, 177–194.
Mandal, N., Samanta, S.K., Bhattacharyya, G., Chakraborty, C., 2003. Deformation of ductile inclusions in a multiple inclusion system in pure shear. Journal of Structural Geology 25, 1359–1370.
Marques, F.O., Coelho, S., 2001. Rotation of rigid elliptical cylinders in viscous simple shear flow: analogue experiments. Journal of Structural Geology 23, 609–617.
Masuda, T., Mizuno, N., 1995. Deflection of pure shear viscous flow around a rigid spherical body. Journal of Structural Geology 17, 1615–1620.
Masuda, T., Michibayashi, K., Ohta, H., 1995. Shape preferred orientation of rigid particles in a viscous matrix: re-evaluation to determine kinematic parameters of ductile deformation. Journal of Structural Geology 17, 115–129.
Montesi, L.G.J., Zuber, M.T., 2002. Parametric analysis of localization during a variety of geological conditions. Journal of Geophysical Research 107, B3. doi:10.1029/2001JB000465.
Moulinec, H., Suquet, P., 2003. Intraphase strain heterogeneity in nonlinear composites: a computational approach. European Journal of Mechanics A Solids 22, 751–770.
Odonne, F., 1994. Kinematic behaviour of an interface and competence contrast: analogue models with different degrees of bonding between deformable inclusions and their matrix. Journal of Structural Geology 16, 997–1006.
Passchier, C.W., Trouw, R.A.J., 2005. Microtectonics. Springer, Berlin, 366 pp.
Pennacchioni, G., Fasolo, L., Cecchi, M.M., Salasnich, L., 2000. Finite element modeling of simple shear flow in Newtonian and non-Newtonian fluids around a circular rigid particle. Journal of Structural Geology 22, 683–692.
Piazolo, S., Bons, P.D., Passchier, C.W., 2002. The influence of matrix rheology and vorticity on fabric development of populations of rigid objects during plane strain deformation. Tectonophysics 351, 315–329.
Regenauer-Lieb, K., Hobbs, B., Yuen, D.A., Ord, A., Zhang, Y., Muhlhaus, H.B., Morra, G., 2006. From point defects to plate tectonic faults. Philosophical Magazine 86, 3373–3392.
Schmid, D.W., Podladchikov, Y.Y., 2004. Are isolated stable rigid clasts in shear zones equivalent to voids? Tectonophysics 384, 233–242.
Taborda, R., Antunesb, J., Marques, F.O., 2003. 2-D rotation behavior of a rigid ellipse in confined viscous simple shear: numerical experiments using FEM. Tectonophysics 379, 127–137.
Takeda, Y.-.T., Griera, A., 2006. Rheological and kinematical responses to flow of two-phase rocks. Tectonophysics 427, 95–114.
ten Grotenhuis, S.M., Passchier, C.W., Bons, P.D., 2002. The influence of strain localisation on the rotation behavior of rigid objects in experimental shear zones. Journal of Structural Geology 24, 485–499.
Tharp, T.M., 1983. Analogies between the high temperature deformation of polyphase rocks and the mechanical behaviour of porous powder metal. Tectonophysics 96, T1–T11.
Treagus, S.H., 2002. Modeling the bulk viscosity of two-phase mixtures in terms of clast shape. Journal of Structural Geology 24, 57–76.

Treagus, S.H., Treagus, J.E., 2001. Effects of object ellipticity on strain, and implications for clast-matrix rocks. Journal of Structural Geology 23, 601–608.
Treagus, S.H., Lan, L., 2000. Pure shear deformation of square objects, and applications to geological strain analysis. Journal of Structural Geology 22, 105–122.
Treagus, S.H., Lan, L., 2003. Simple shear of deformable square objects. Journal of Structural Geology 25, 1993–2003.
Tullis, T.E., Horowitz, F.G., Tullis, J., 1991. Flow laws of polyphase aggregates from end-member flow laws. Journal of Geophysical Research 96, 8081–8096.
Wilson, C.J.L., 1983. Foliation and strain development in ice-mica models. Tectonophysics 92, 93–122.